Journal of Materials Chemistry C

Accepted Manuscript

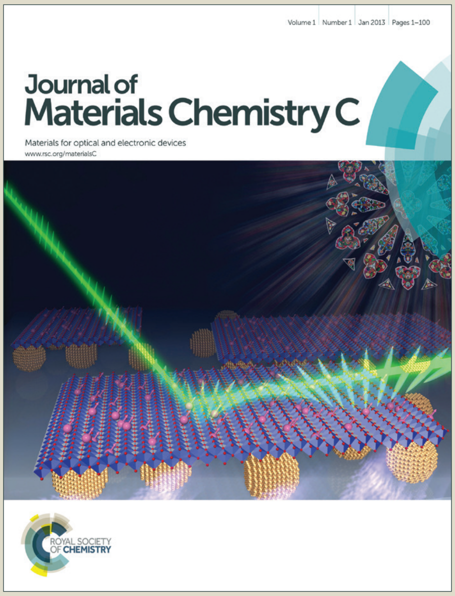

ROYAL SOCIETY OF CHEMISTRY

www.rsc.org/materialsC

Carbon-Metal Nanosheets from the Water-Hexane Interface

*Hicham Hamoudi**

International Center for Materials Nanoarchitectonics (WPI- MANA), National Institute for Materials Science (NIMS), 1-1 Namiki, Tsukuba, 305-0044, Japan

*** Corresponding author**

Corresponding authors: Hicham Hamoudi: Phone: +81-29-851-3354 (ext.8672), FAX: +81-29-860-4706,

E-mail: Hamoudi.hicham@nims.go.jp
hichamhamoudia@gmail.com

Abstract:

This report describes a new approach to prepare atoms thick metal–sulfide–graphene nanosheets produced by subsequent annealing of crosslinked carbon–metal film formed at the water–hexane interface. A bipyridine dithiol (BPD) layer self-assembled at the water–hexane hydrophilic/hydrophobic biphasic medium was used to encapsulate metal ions (M^{+2}) (M = Co or Ni). Subsequently, the BPD-M^{+2} film was crosslinked using UV-light. Then the resulting carbon–metal nanosheets were annealed at high temperature under N_2, transforming these molecular sheets into a homogeneous nano-crystalline metal–sulfide–graphene hybrids (MSGH). This approach can produce semi-transparent conducting films having marked conductivity dependence on the number of the nanosheets in a stack. The suggested strategy opens broad prospects toward the MSGH architecture using a simple process with new properties for new applications such as energy conversion/storage and electronics.

Subject terms: Self-Assembly, water–hexane interface, metal–sulfide–graphene nanosheets

1-Introduction

Graphene, regarded as a perfect example of a two-dimensional electron system, presents tremendous possibilities for engineers because of its exceptional electrical, magnetic, and optical properties.[1–4] In recent years, increasing interest has surrounded the development of graphene. Different methods are useful for graphene preparation on metallic surfaces: (i) elevated temperature segregation of carbon atoms to the surface of a bulk metallic sample doped with carbon before treatment (ii) and thermal decomposition of molecules containing carbon on the surface of a transition metal, involving the cracking of light hydrocarbon molecules.[1, 5]

Different theoretical studies have been conducted to demonstrate the wide range of application of metal–graphene hybrids. Nevertheless, very little experimental work has been reported.[1] Instability and the nonhomogeneous distribution of the metal nanostructure on graphene remain as obstacles hindering the development of these 2D materials.[1] Engineering graphene using adsorbates such as transition metals can control the ground state and magnetic properties of the graphene.[6] Several strategies might be used to enable the modification of the electronic structure of the graphene: (1) modification of the edge, the so-called nanoribbons[7]; (2) modification of the electronic structure by interaction with substrates[8, 9]; (3) multilayer graphene[10, 11] ; and (4) deposition of metal ore molecules on top of the graphene.[12, 13] Are there ways to generate stable nanocrystalline metal-doped graphene hybrids using a simple process? Although numerous studies have examined graphene, no report in the literature has described the experimental preparation of nanocrystalline doped-graphene on a liquid–liquid interface

As early as 1930, Langmuir and Blodgett assembled molecules on a water surface to form membranes known as Langmuir–Blodgett (LB) films.[14] The Langmuir–Blodgett molecular monolayer presents similarities to biological membranes, where lipids self-organize via their intramolecular interaction. Air–liquid and liquid–liquid interfaces such as air–water and water–hexane are useful for ordering a monolayer of molecules via spontaneous formation.[15, 16] The exposure of molecular interfaces to UV irradiation crosslinked the monolayer and polymerized the film.[16] Crosslinking the LB molecular films using UV light might transform them into a robust nanosheet. Different experiments in which the monolayer was cross-linked after transfer to a solid substrate have already been reported.[17, 18] Nanometer carbon membranes are useful for potential applications including fuel cells, biological macromolecule separation, sensors, and optical devices.[19] Very thin carbon sheets are readily produced by crosslinking the self-assembled monolayer on a metallic substrate and then peeling it off the substrate.[20, 21] An important shortcoming is that the sheets are often damaged during peeling and transfer to other supports.[21]

Metal sulfide is regarded as an efficient catalytic substance. The metal–sulfide–graphene nanocomposite was proposed as a potential transparent conductive oxide-free counter electrode materials with high electrocatalytic activity for different applications.[22]

This report presents a new method to generate nanocrystalline metal–sulfide–graphene hybrids (MSGH) using an internal metal source based on a sequence of UV radiation and thermal treatment of the (5,5'-Bis (mercaptomethyl)-2,2'-bipyridine)-M^{+2} layer (BPD-M^{+2}, M=Ni or Co). First the BPD-M^{+2} is self-assembled at the water–hexane interface, thereby forming a monolayer. Subsequent exposure of the monolayer to UV light engenders the formation of the freestanding carbon–metal–sulfide nanosheet (CMSNS). Then annealing the CMSNS under N_2 provides the MSGH nanocomposite. The CMSNS and the MSGH were characterized using various complementary techniques. The MSGH conductivity displays a metallic behavior that can be useful for different electronics applications. Similarly, the stability and the homogeneous distributions of the metal-sulfide particles on the carbon nanosheet are expected to open new vistas for oxygen reduction reactions, energy conversion/storage, and electronics technologies.[22–25]

2-Methods

5,5’-Bis (mercaptomethyl)-2,2’-bipyridine BPD was purchased from Aldrich Chemical Co. Inc. and was then used as received. The monolayer of the 5,5’-bismercaptomethyl-2,2’-bipyridine (BPD) was prepared by mixing water that had been freshly degassed by N_2 bubbling with a fresh solution of BPD on *n*-hexane. Well-degassed solutions by Ar have been used. After formation of the water–hexane deoxygenated interface, all preparation steps were performed in the absence of ambient light to avoid oxidation of the thiol groups. A concentrated (0.05 M) $CoCl_2$ or $NiCl_2$ aqueous solution was added to the interface to form the Tris(5,5’-bismercaptomethyl-2,2’-bipyridine)metal(II) layer (Figure 1 shows the proposed structure). Exposition of the film to UV (Xe polychromatic lamp, 1.82 w/cm^2) caused lateral crosslinking of the BPD-M^{+2} layer, as depicted in Figure 1.

The BPD self-assembled monolayer (SAM) on gold was used as a reference system to elucidate the morphology of the BPD monolayer formed at the liquid–liquid interface. The BPD SAM was prepared by immersing the gold support into a freshly prepared 1 mM solution of n-hexane for 1 h at approximately 60 °C. We used solutions that had been well degassed using Ar. All preparation steps were performed in the absence of ambient light, following the same protocol as that used in our previous studies.[26]

All XPS measurements were conducted at the MANA Foundry using a spectrometer (XPS Alpha 110 mm; Thermo Fisher Scientific Inc.). The XPS spectra in the S 2p, C 1s, N 1s, and Co 2p regions were recorded. The spectra acquisition was performed in normal emission geometry using Al Kα α radiation. The binding energy (BE) scale of each spectrum was calibrated individually to the Au $4f_{7/2}$ emission at 83.95 eV. Wide angle thin-film X-ray diffraction (XRD) patterns were obtained with a Rigaku smartlab diffractometer using monochromated CuKa radiation (40 kV, 40 mA) at a scanning rate of 0.5° min^{-1}.

A UV/Vis/NIR spectrophotometer (V-570; Jasco Corp.) was used to measure the UV/Vis transmission mode.

The AFM topographical and phase images were collected using an SPM microscope (diMultimode; Veeco Instruments) and NanoScope software in tapping mode. Before measuring the thickness, the SPM was calibrated using a calibration reference consisting of a silicon substrate having a regular series of pits, each 180 nm deep, plated with platinum.

To measure the film thickness, the freely suspended membrane was placed on the silicon wafer. Its edge area was scanned.

The membrane morphology was investigated using a scanning electron microscope (S-4300; Hitachi Ltd.) equipped with a W tip cold-FE electron emitter. Then TEM observations and EDX were performed using a TEM system (JEM-2010; JEOL) operated at 200 kV.

3-Results and discussion

In actuality, π-congregated molecules can self-assemble spontaneously because of the combination of different interactions such as π stacking, van der Waals, and H-bonding interactions.[27] The exposure of the tris-BPD-M^{+2} film formed on the water–hexane interface to UV light of approximately 5 min engenders the formation of a crosslinked nanosheet. The nanosheet is transparent, but it exhibits a clear Tyndall effect because of side-incident light scattering by the carbon–metal–sulfide nanosheet (CMSNS) formed at the water–hexane interface (see Figure 2a). It is noteworthy that without exposition of the SAM to UV, no nanomembrane formation occurs, except after long formation of a dense aggregate. Figure 2(b) presents a TEM image of the nanosheet deposited on a TEM grid. The CMSNS has large lateral dimensions of approximately 5 cm^2. The CMSNS shows good resistivity to an electron beam of 200 keV. In some cases, 2D material electron beams can induce dramatic structural changes and radiation damage, which presents an obstacle to obtaining the desired information in imaging and chemical analysis in the TEM.

3.1-Carbon–Cobalt Nanosheet

Figure 3 depicts a TEM micrograph of the CMSNS edge on the TEM grid, in addition to elemental maps of C, Co, S, and N (denoted respectively by red, magenta, yellow, and green dots) of the CMSNS. The results show homogenized distributions of both S and Co on the nanosheet. Additionally, it is noteworthy that 49 wt% of S and 8.19 wt% of Co were detected in the composite.

The CMSNS was well cleaned in water before transfer to the SiO_2 substrate. Thereafter, the CMSNS was characterized using X-ray photoelectron spectroscopy (XPS), XRD, UV–Vis, and high-resolution transmission electron microscopy (HRTEM).

The C 1s, N 1s, S 2p, and Co 2p XPS spectra of the CMSNS, compared with the BPD self-assembled monolayer (SAM) on gold (111), are presented in Figure 4. The C 1s spectra of the BPD SAM and the BPD-Co nanosheet are portrayed in Figure 4(a). The main peak at 285.5 eV of the BPD SAM is a superposition of contributions from two carbons: The C directly bound to the nitrogen atoms (red curve), and the C of the aliphatic moieties not-bound to the nitrogen in the pyridine unit (blue curve).[27] The C 1s of the BPD-Co nanosheet on SiO_2 shows a similar composition to that of C 1s of BPD SAM on gold.

The N 1s XPS spectra of the BPD SAM are displayed in Figure 4(c). A single symmetric peak at 399 eV is assigned to the nitrogen in the pyridine rings. For N 1s spectra of the CMSNS (Figure 4-c), the presence of Co^{+2} on the molecular backbone produces a chemical shift of the main peak towards a higher binding energy by 1.2 eV, which is a fingerprint of the binding of the bipyridine sites to the Co^{+2} moiety. [21, 28] The shift described in an earlier report[21] was more pronounced than in this study, probably because of the formation of the Co-tris-bipyridine complex (see Figure 1), where N in this case is less electropositive than the N in an Ni-bi- bipyridine system.

The spectral deconvolution of the S 2p BPD SAM (Figure 4-b) was done by setting a 1.2 eV $2p_{1/2,\ 3/2}$ splitting and introducing two doublets: one at 162 eV commonly assigned to the thiolate-Au species and the other at about 163.5 eV corresponding to sulfur of the free thiol (SH) groups or S–S bonds. The S 2p of the CMSNS shows a main peak at 163.5 eV assigned to the free thiol (SH or S–S), which excludes the probability of formation the binding of Co to SH because of the short exposition to the Co solution (5 min). [21, 26, 28–31]

Figure 4(d) shows the Co 2 $p_{3/2}$ region. The peak at 780.5 eV is assigned to Co^{+2}. The shake-up structure (“s” in the figure) and the energy separation of 15.6 eV between the 2 $p_{3/2}$ and 2 $p_{1/2}$ peaks are consistent with divalent cobalt.[38, 39]

The BPD film thickness was evaluated based on the I_{C1s} / I_{Au4f} intensity ratios assuming a standard exponential attenuation of the photoelectron signal and using the attenuation lengths reported by Lamont and Wilkes.[32] As calibration references, the dodecanethiol (DDT)/Au sample of known thickness were used assuming that this sample has comparable packing densities to those of the BPD films. The BPD SAM is ca. 2.1 ± 0.3 nm, which shows good agreement with the BPD molecule height.[21, 28] The nanosheet thickness determined using AFM was approximately 2.5 nm for the CMSNS (see Figure 5a), this thickness is the same as a molecular length, indicating that the molecules are oriented as nearly perpendicular to the interface and that they are nearly all-trans.

The UV–Vis measurement shown in Figure 5b exhibits characteristic metal-to-ligand charge-transfer (MLCT) bands. The complex has an absorption maximum in the UV region in both oxidation states: $\lambda_{\max}(\varepsilon)$ = 346, 250 nm for CMSNS. These bands are attributed to the intraligand $\pi \rightarrow \pi^*$ transition.[33]

A millimeter lateral dimension range of CMSNS was annealed under N_2 at temperatures up to 600 °C for 20 min. A carbon hybrid layer MSGH was produced. It is noteworthy that a few amorphous carbon hybrid layers MSG can be generated at low annealing temperatures of less than 400 °C. Figure 5c displays an AFM image of a monolayer MSGH (600 °C) deposed on a SiO_2 substrate. The layer thickness measured using AFM is approximately 1.3 nm, which typically corresponds to a monolayer of graphene.[34, 35] The noise in the thickness evaluation on Figure 5c is probably related to the metal nanoparticle contribution and to defects in the annealed nanosheet. The chemical composition of the MSGH on SiO_2 substrate is shown in Figure 4. High background in the S 2p spectrum of the MSGH hinders analysis of the spectra. That background is attributable to the influence of the Si (2s) peak located in the region between 150 eV and 155 eV. Spectra of the former films exhibit different distinct features. The main broad and distinctly asymmetric peak at 164 eV is probably a superposition of the contributions from the Co–thiolate species and the (S–S) linkages or free thiol groups SH, whereas the second located at 168.00 leV is probably associated with the sulfur atom bonded to the oxygen.[21, 26, 29]

The XPS N 1s spectra show a chemical shift of the main peak in the direction of the low binding energy 399.11 eV, which is a fingerprint of the decoupling of the Co^{+2} from the bipyridine sites.[21, 28] A feature located at 401.5 eV attributes to the N-graphene structure.[36, 37] Actually, C1s consists of component peaks corresponding to different carbon species C–C and C=C (presented on the blue line in Figure 4a), C–N (red line), and C=O (magenta line). The Co 2 $p_{3/2}$ XPS region shows a new shoulder at 779 eV assigned to the Co^0 metal form (Figure 4).[38, 39]

Figure 6 shows XRD patterns of the MSGH nanocomposites deposed on a gold substrate. The two main peaks at 2 theta 38.21 and 44.55 correspond to the Au (Pdf 00-001-1172), the remainder of diffraction peaks are consistent with the values given in the standard Pdf cards for Co (Pdf 00-001-1259), CoS2 (Pdf 00-041-1471), Co9S8 (Pdf 00-056-1288), and ω-S (Pdf 00-020-1227). The reflection peak of graphitic carbon is weak, possibly because the disordered graphene structure is obtained.

The MSGH structure was characterized using transmission electron microscopy TEM and Raman spectroscopy. Figure 7 exhibits the TEM, HRTEM, elemental maps, and EDX of the MSGH. The elemental maps (Figure 7c) of sulfur and cobalt confirmed that the bright particles in the TEM image in Figure 7a are cobalt and cobalt–sulfur particles, probably formed by segregation of the cobalt and sulfur on the top of the MSGH after annealing. Energy-dispersive X-ray (EDX) microanalysis revealed an important sulfur peak, which is around twice that of cobalt, as shown in Figure 7d.

Figures 7a and 6b show a room temperature STEM image and HRTEM images of the monolayer MSGH with their selected area electron diffraction, including the related EELS spectra. The STEM micrograph in Figure 7a shows a homogeneous distribution of the metal and metal sulfide nanoparticles on the MSGH sheet. At high HRTEM magnification (Figure 7b), it is readily apparent that ordered graphene areas with lateral demotions of 10–15 nm have formed. The well-defined hexagonal honeycomb structure in Figure 7b and the electron diffraction pattern in Figure 7b confirm a hexagonal symmetry of the graphene areas. The graphene areas at the edges are altered with Co and Co-S domains, as shown in Figure 7b. The coalescence between the nanocrystals is apparent in high-resolution TEM images. The EELS spectrum taken of the same area shows a clear peak of Co. The XPS, XRD, EDX, and EELS spectroscopies of the MSGH confirm the TEM observation regarding the formation of CoS and Co nanostructure on the annealed nanosheet.

Figure 8a portrays a Raman spectrum of multilayer nanosheet of the Co-sulfide graphene on SiO_2 (measured using an excitation wavelength of 532 nm). The single-sheet Raman spectra shows graphitization confirmed by D (1365 Cm^{-1}) and G at Γ (1587 Cm^{-1}) peaks.[1] Similar Raman spectra have been reported on different carbon nanomembrane prepared on the metal substrate and doped graphene.[20, 40] The

D band is associated with the loss of lattice symmetry. Symmetry breaking can result from any of the following: (i) presence of vacancies and interstitials; (ii) introduction of interfaces at the borders of the crystalline areas; or (iii) substitution atoms that can also be introduced intentionally, for instance by ion implantation.[1] In addition, the G band shows prominent Raman features in graphene and graphite.

Increasing the number of sheets in a stack causes increased D and G band intensities, and splitting of the G peak into a doublet structure G1 and G2 (Figure 8a). Splitting in the G peak observed in the Raman spectra of graphene and other disordered sp^2 carbon materials usually occurs because of graphite intercalation compounds (GICs).[40, 41] Characteristics of the G band in the GIC are known to be affected by three factors: intercalate coupling, change in the lattice constant, and charge transfer.[41, 42] Figure 5b shows a red shift of the G_2 peak compared with the G_1 peak. A similar downward shift was observed for the *n*-doped multilayer graphene film.[42, 6]

The electrical properties of the Co–S–Graphene nanosheet were investigated as a function of the number of layers in a stack. Multisheet films are formed by deposition of alternating layers. Figure 8b presents I–V characteristics using four probes arranged equidistantly in a line and contacted the nanosheets. The I–V curve of the single Co–S–G nanosheet remains linear, showing metallic behavior. Here, the sheet resistivity ρ_s was measured using the following formula.[43]

$$\rho_s = \frac{\pi}{\ln(2)} \frac{V}{I}\ \Omega/\text{square}$$

At bias voltage of 1 V, ρ_s corresponds to 179 $k\Omega sq^{-1}$ demonstrating the clear metallic characteristics of the film. The resistivity drops to 61.7 $k\Omega sq^{-1}$ as the number of layers increases to three nanosheets, producing 100 times lower sheet resistivity than that of single chemically reduced graphene oxide sheets,[44] and 10 times higher resistivity than that of the free graphene monolayer.[45] The conductivity increases with the increase of the number of the sheets, which shows good agreement with the Raman experiment when the charge transfer and the concentration of the sp2 carbon nanostructures increase under the same conditions. This variation can be attributed to changes in the electronic structure of the system, where the thickness increase is accompanied by an important degree of electron delocalization in the system.[30]

3.2-Carbon–Nickel Nanosheet

Additional metal ions have been tested as an internal dopant source such as nickel. The surface morphology of the hybrid structure carbon–nickel–sulfide nanosheet (C-Ni-SNS) after annealing is shown in the HRTEM image (Figure 9a), which exhibits the same behavior as that of the Co case. Bright nanoparticles (NPs) are formed uniformly over the entire surface of nanosheet flakes. The mean particle sizes are between 50 nm and 15 nm. Figures 9b and 9c respectively show a TEM micrograph and elemental maps of sulfur and nickel in the annealed CMSNS. The red dots in Figures 9(c) show sulfur; the green dots show nickel. The elemental maps show that the bright particles in Figure 9a are Ni and Ni–S NPs which is in good agreement with the Co-S-G results. Figure 9d shows high-resolution image lattice planes of Ni NP. The high crystallinity of NPs is confirmed by the electron diffraction pattern in Figure 9e.

It is particularly interesting that the average diameter of the Co/CoS particles is approximately 5 nm. However, Ni/NiS particles have sizes in the range of approximately 50–15 nm. This size difference is probably attributable to different phenomena related to the morphology and the properties of the metal ions in the SAM. This phenomenon is under investigation and remains the subject of future studies.

4-Conclusion

In conclusion, this report presented a novel method to produce metal–sulfide graphene nanosheets at a liquid–liquid interface. After crosslinking of (BPD-Co^{+2}) SAMs using UV light on the water–hexane interface, the CMSNS were transferred to the SiO_2 substrate. Using a combination of several complementary experimental techniques, the chemical properties of the CMSNS nanomembrane were investigated. The salient benefit of this technique lies in using the encapsulated metals and the sulfur end group on the CMSNS backbone as an internal doping source, providing homogeneous metal–sulfide nanostructures that are covalently bonded to graphene after the nanosheet annealing process. Using an external metallic source for metal-doped graphene such as metal sputtering provides nonhomogeneous metallic distribution, and also an unstable configuration of the metal on the top of the graphene.[1] In the present study, the heating process of the CMSNS stimulates aggregation of the metallic ions. Together with the sulfur, they provide metal hybrid nanostructures. Different nitrogen sites on the carbon nanosheet reinforce the metallic nanostructure stability. The approach is useful to prepare extremely large and complex metallographene heterostructures with attractive properties based on an extremely simple method at the liquid–liquid interface. Further studies for applications in various fields of these new nano-carbon materials are in progress at our institute, especially for electronics, and for energy conversion and storage.

Acknowledgments: I appreciate the valuable assistance of MANA foundry. This work was supported by the International Center for Young Scientists (ICYS) on Materials Nanoarchitectonics (WPI –MANA).

References

1. Raza, H. Graphene Nanoelectronics: Metrology, Synthesis, Properties and Applications. *Springer* **2012**.
2. Schwierz, F. Graphene transistors. *Nature Nanotechnology* **2010**, *5*, 487–496.
3. Wang, Y.; Huang, Y.; Song, Y.; Zhang, X.; Ma, Y.; Liang, J.; Chen, Y. Room-Temperature Ferromagnetism of Graphene. *Nano Lett*. **2009**, *9*, 220.
4. Geim, A. K. Graphene: Status and Prospects. *Science* **2009**, *324*, 1530.
5. Turchanin, A.; Weber, D.; Bueenfeld, M.; Kisielowski, C.; Fistul, M. V.; Efetov, K. B.; Weimann, T.; Stosch, R.; Mayer, J.; Gölzhäuser, A. Conversion of Self-Assembled Monolayers into Nanocrystalline Graphene: Structure and Electric Transport. *ACS Nano* **2011**, *5*, 3896–3904.
6. Giovannetti, G.; Khomyakov, P. A.; Brocks, G.; Karpan, V. M.; J. van den Brink; Kelly, P. J. Doping Graphene with Metal Contacts. *Phys. Rev. Lett*. **2008**, *101*, 026803.
7. Bai, J.; Cheng, R.; Xiu, F.; Liao, L.; Wang, M.; Shailos, A.; Wang, K. L.; Huang, Y.; Duan, X. Very large magnetoresistance in graphene nanoribbons. *Nat Nanotechnology* **2010**, *5*, 655–659.
8. Zhou, S. Y.; Siegel, D. A.; Fedorov, A. V.; Gabaly, F.El; Schmid, A. K.; Castro Neto, A. H.; Lee, D.-H. Origin of the energy bandgap in epitaxial grapheme, & A. Lanzara. *Nat. Mater*. **2008**, *7*, 259.

9. Rotenberg, E.; Bostwick, A.; Ohta, T.; McChesney, J. L.; Seyller, T.; Horn, K. Origin of the energy bandgap in epitaxial grapheme. *Nat. Mater*. **2008**, *7*, 258.
10. Ohta, T.; Bostwick, A.; Seyller, T.; Horn, K.; Rotenberg, E. Controlling the Electronic Structure of Bilayer Graphene. *Science* **2006**, *313*, 951.
11. Zhang, Y.; Tang, T.-T.; Girit, C.; Hao, Z.; Martin, M. C.; Zettl, A.; Crommie, M. F.; Shen, Y. R.; Wang, F. Direct observation of a widely tunable bandgap in bilayer grapheme. *Nature* **2009**, *459*, 820.
12. Chan, K. T.; Neaton, J. B.; Cohen, M. L.. First-principles study of metal adatom adsorption on grapheme. *Phys. Rev*. B **2008**, *77*, 235430.
13. Coletti, C.; Riedl, C.; Lee, D. S.; Krauss, B.; Patthey, L.; von Klitzing, K.; Smet, J. H.; Starke, U. Charge neutrality and band-gap tuning of epitaxial graphene on SiC by molecular doping. *Phys. Rev*. B **2010**, *81*, 235401.
14. Blodgett, K. B. *USA Patent* **1940**, 2220860.
15. Tikhonov, A. M.; Schlossman, M. L.. Surfactant and Water Ordering in Triacontanol Monolayers at the Water–Hexane Interface. *J. Phys. Chem*. B **2003**, *107*, 3344–3347.
16. Wilson, T. E.; Bednarski, M. D. Polydiacetylene monolayers functionalized with amino acids, *Langmuir* **1992**, *8*, 2361.
17. Goedel, W. A.; Heger, R. Elastomeric Suspended Membranes Generated via Langmuir−Blodgett Transfer. *Langmuir* **1998**, *14*, 470–3474.
18. Christi, P.; Petty, M. C.; Robert, G. G.; Richards, D. H.; Service, D.; Stewart, M. J. The preparation and dielectric properties of polybutadiene Langmuir-Blodgett films *Thin Solid Films* **1985**, *134*, 75.

19. Baker, R. W. Membrane Technology and Applications (Wiley, Hoboken, 2004).
20. Turchanin, A. Gölzhäuser, A. Carbon nanomembranes from self-assembled monolayers: Functional surfaces without bulk, Progress in Surface Science, 2012, 87 (5), 108-162
21. H. Hamoudi, Bottom-up nanoarchitectonics of two-dimensional freestanding metal doped carbon nanosheet, RSC Advences 2014, 4, 22035-22041

22. Hui Bi, Wei Zhao, Shengrui Sun, Houlei Cui, Tianquan Lin, Fuqiang Huang, Xiaoming Xie, Mianheng Jiang. Graphene films decorated with metal sulfide nanoparticles for use as counter electrodes of dye-sensitized solar cells. Carbon,

2013, 61, 116-123.

23. Rajesh Kumar, Hyun-Jun Kim, Sungjin Park, Anchal Srivastava, Il-Kwon Oh. Graphene-wrapped and cobalt oxide-intercalated hybrid for extremely durable super-capacitor with ultrahigh energy and power densities. Carbon, 2014, 79, 192-202.

24. Qiang Li, Zhian Zhang, Zaiping Guo, Yanqing Lai, Kai Zhang, Jie Li, Improved cyclability of lithium–sulfur battery cathode using encapsulated sulfur in hollow carbon nanofiber nitrogen-doped porous carbon core–shell composite. Carbon, 2014, 78, 1-9

25. Da-Wei Wang, Qingcong Zeng, Guangmin Zhou, Lichang Yin, Feng Li, Hui-Ming Cheng, Ian R. Gentle, Gao Qing Max Lu. Carbon–sulfur composites for Li–S batteries: status and prospects. J. Mater. Chem. A, 2013,1, 9382-9394

26. Hamoudi, H.; Döring, K.; Chesneau, F.; Lang, H.; Zharnikov, M. Self-Assembly of Pyridine-Substituted Alkanethiols on Gold: The Electronic Structure Puzzle in the Ortho- and Para-Attachment of Pyridine to the Molecular Chain. *J. Phys. Chem.* C **2012**, *116*, 861–870.
27. Mammen, M.; Choi, S.-K.; Whitesides, G. M. *Angew. Chem.* **1998**, *110*, 2908–2953; *Angew. Chem. Int. Ed.* **1998**, *37*, 2754–2794.
28. H. Hamoudi, Crossbar nanoarchitectonics of the crosslinked self-assembled monolayer. Nanoscale res let, 2014, 9(1), 1-7

29. Hamoudi, H.; Döring, K.; Chesneau, F.; Lang, H.; Zharnikov, M. Self-Assembly of Pyridine-Substituted Alkanethiols on Gold: The Electronic Structure Puzzle in the Ortho- and Para-Attachment of Pyridine to the Molecular Chain. *J. Phys. Chem.* C **2012**, *116*, 861–870.
30. Hicham Hamoudi, Kohei Uosaki, Katsuhiko Ariga, Vladimir A Esaulov, Going beyond the self-assembled monolayer: metal intercalated dithiol multilayers and their conductance. RSC Advances, 2014,4, 39657-39666

31. Pasquali, L.; Terzi, F.; Seeber, R.; Nannarone, S.; Datta, D.; Dablemont, C.; Hamoudi, H.; Canepa, M.; Esaulov, V. A.UPS, XPS, and NEXAFS Study of Self-

Assembly of Standing 1,4-Benzenedimethanethiol SAMs on Gold. *Langmuir* **2011**, *27*, 4713– 4720.

32. Lamont, C. L. A.; Wilkes, J. Attenuation Length of Electrons in Self-Assembled Monolayers of n-Alkanethiols on Gold. Langmuir 1999, 15, 2037

33. C. S. Pilz and C. Steinem, Modulation of the conductance of a 2,2′-bipyridine-functionalized peptidic ion channel by Ni^{2+}. Eur. Biophys. J., 2008, 37, 1065–1071

34. Gupta, A.; Chen, G.; Joshi, P.; Tadigadapa, S.; Eklund, P. C. Raman scattering from high-frequency phonons in supported n-graphene layer films. Nano Lett. 2006, 6 (12), 2667–2673.

35. Li, X.; Wang, X.; Zhang, L.; Lee, S.; Dai, H. Chemically Derived, Ultrasmooth Graphene Nanoribbon Semiconductors. Science 2008, 319 (5867), 1229–1232.

36. Xiaolin Li, Hailiang Wang, Joshua T. Robinson, Hernan Sanchez, Georgi Diankov, and Hongjie Dai, Simultaneous Nitrogen Doping and Reduction of Graphene Oxide. J. AM. CHEM. SOC. 2009, 131, 15939–15944

37. Hongliang Peng, Zaiyong Mo, Shijun Liao, Huagen Liang, Lijun Yang, Fan Luo, Huiyu Song, Yiliang Zhong, Bingqing Zhang, High Performance Fe- and N- Doped Carbon Catalyst with Graphene Structure for Oxygen Reduction. Scientific reports3 : 1765 | DOI: 10.1038/srep01765

38. Wagner, C. D.; Riggs, W. M.; Davis, L. E.; Moulder, J. F.; Muilenberg, G. E. Handbook of X-Ray Photoelectron Spectroscopy (Perkin-Elmer Corporation, Physical Electronics Division, Eden Prairie, 1979).
39. N.S. McIntyre, M. G. Cook, al. X-ray photoelectron studies on some oxides and hydroxides of cobalt, nickel, and copper. Anal. Chem. 1975, 47, 2208

40. Xie, J.; Liu, S.; Cao, G.; Zhu, T.; Zhao, X. Self-assembly of CoS2/graphene nanoarchitecture by a facile one-pot route and its improved electrochemical Li-storage properties. *Nano Energy* **2013**, *2*, 49–56.
41. Zhan, B. D.; Sun, L.; Ni, Z. H.; Liu, L.; Fan, X. F.; Wang, Y.; Yu, T.; Lam, Y. M.; Huang, W.; Shen, Z. X. FeCl 3-Based Few-Layer Graphene Intercalation

Compounds: Single Linear Dispersion Electronic Band Structure and Strong Charge Transfer Doping Adv. *Funct. Mater*. **2010**, *20*, 3504–3509.

42. Das, B.; Voggu, R.; Routa, C. S.; Rao, C. N. R. Changes in the electronic structure and properties of graphene induced by molecular charge-transfer. *Chem. Commun*. **2008**, 5155–5157.

43. Plummer, J. D.; Deal, M. D.; Griffin, P. B., In Silicon VLSI Technology Prentice Hall: Upper Saddle River, NJ, USA, 2000; p 114.

44. Marco Sangermano, Sophie Marchi, Luca Valentini, Silvia Bittolo Bon, Paola Fabbri, Transparent and Conductive Graphene Oxide/Poly(ethylene glycol) diacrylate Coatings Obtained by Photopolymerization. Macromolecular Materials and Engineering, 2011, 296, 401–407

45. K. S. Novoselov, A. K. Geim, S. V. Morozov, D. Jiang, M. I. Katsnelson, I. V. Grigorieva, S. V. Dubonos, A. A. Firsov, Two‑dimensional gas of massless Dirac fermions in graphene. Nature 2005, 438 , 197.

Figure 1. Preparation of freestanding nanosheet. (a) Self-assembly monolayer of the Tris-BPD-Co on the water–hexane interface, and the configuration proposal of Tris-BPD-Co layer after crosslinking using UV. (b) Freestanding carbon–metal–sulfide nanosheet from the water hexane interface.

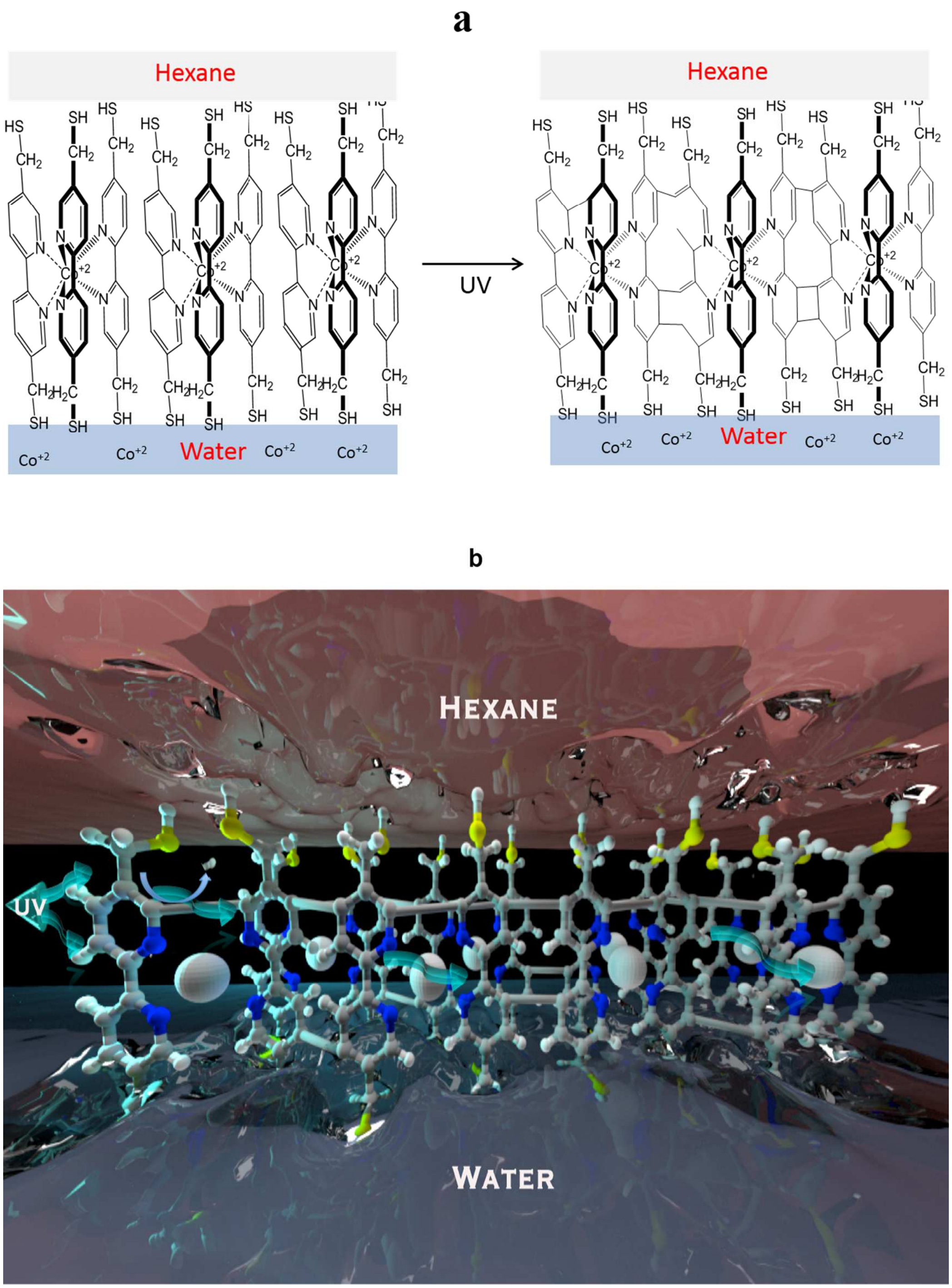

Figure 2. Optical property and TEM image of the nanosheet (a) Tyndall light scattering on the CMSNS formed at the water–hexane interface, (b) TEM image of the CMSNS deposited on TEM grid.

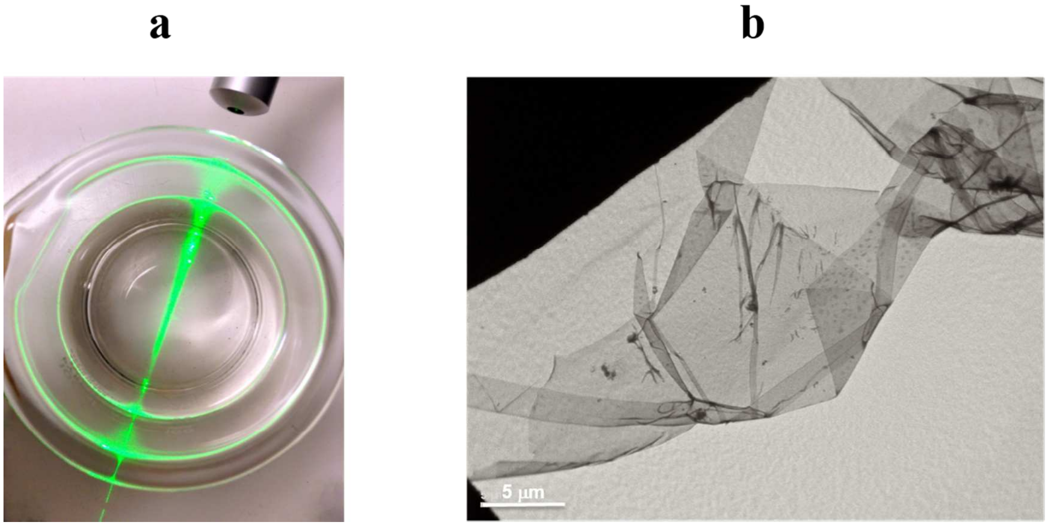

Figure 3. TEM and Elemental map of the sheet (a) TEM image of the CMSNS edge, and elemental map of C (b), Co (c), S (d), and N (e) of the CMSNS.

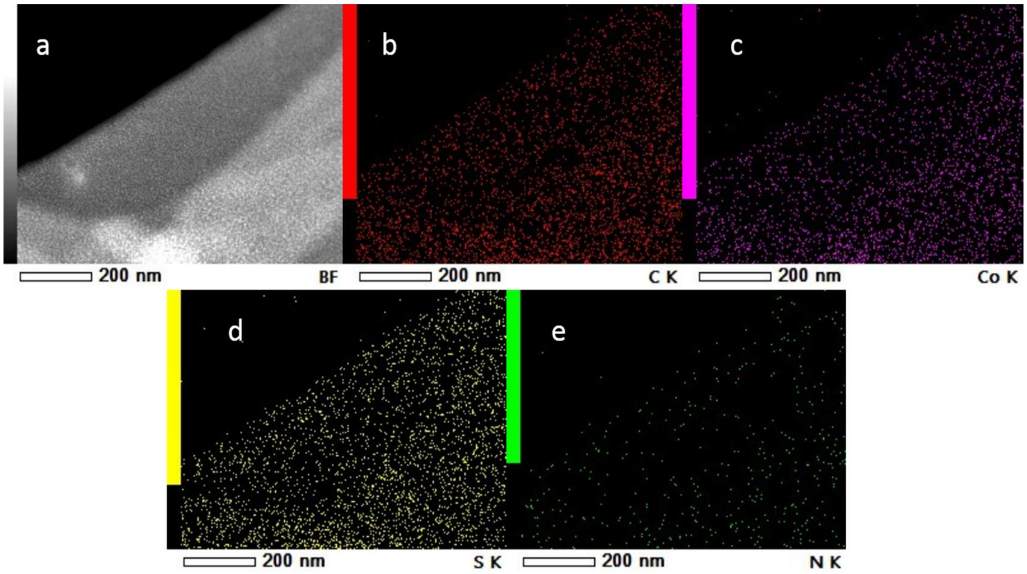

Figure 4. Chemical composition of the nanosheet and the graphene hybrid materials. XPS C 1s, N 1s, S 2p, and Co 2p spectra of the BPD on gold, BPD-Co layer on SiO_2, and the annealed BPD-Co layer on SiO_2 at 600 °C. Some spectra are decomposed into the individual contributions related to different species; see the text for details.

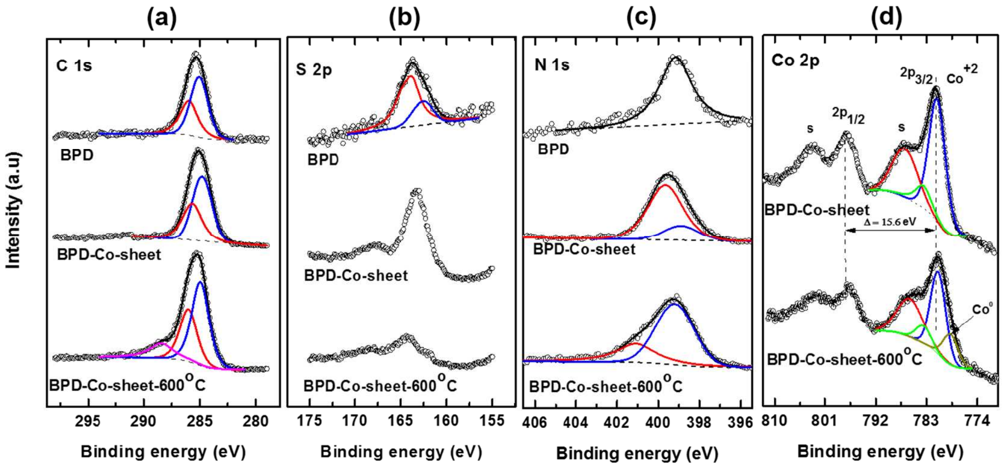

Figure 5. AFM and UV-Vis properties of the sheet. (a) AFM image of the CMSNS on SiO_2. (b) UV-vis spectra of the CMSNS deposited on a SiO_2.(c) AFM image of the MSGH on SiO_2.

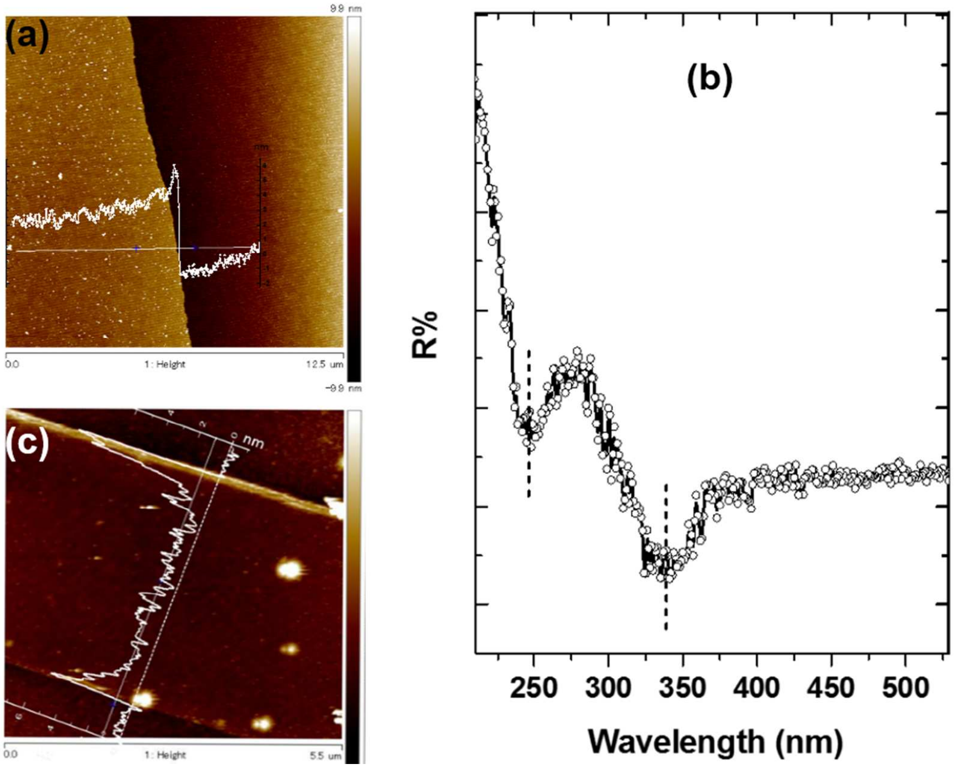

Figure 6. XRD patterns of CoS-graphene composites on Au substrate.

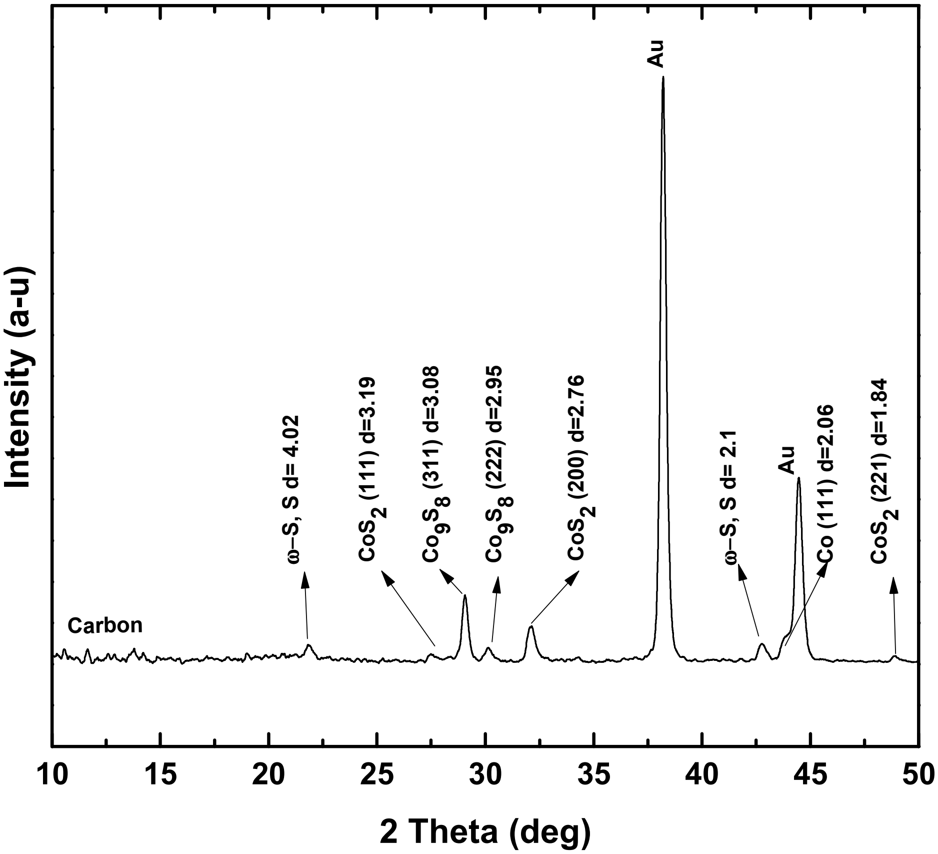

Figure 7. TEM of the annealed sheet. (a) STEM micrograph of the annealed CMSNS deposited on the TEM grid, (b) nanoscale HRTEM image of the annealed CMSNS with the EELS spectra and selected area electron diffraction pattern of the crystalline Co–S–graphene nanocomposite. (c) TEM image of the annealed CMSNS and elemental map of carbon, sulfur, and cobalt, (d) C, S, and Co EDX of the annealed sheet, the intense red peaks related to the Cu of the TEM grid.

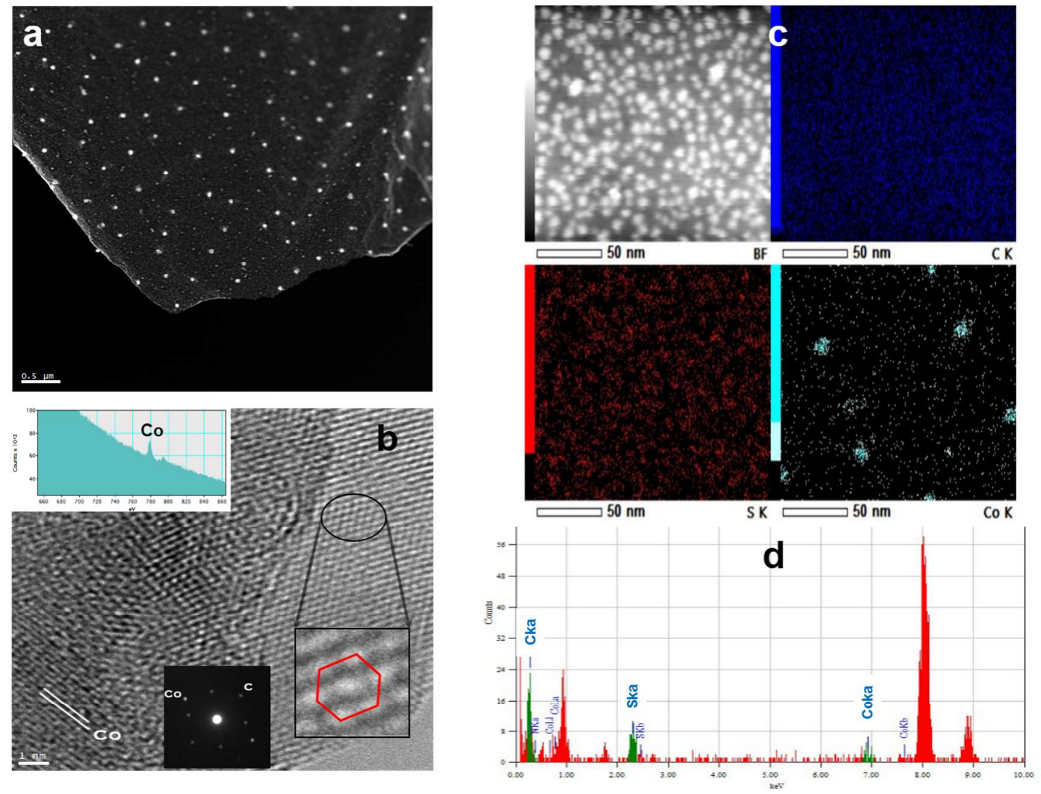

Figure 8. Raman shift and fore probes IV characteristics of the annealed nanosheet. (a) Raman shift of the annealed CMSNS, and (b) Room temperature fore probes current versus voltage of the annealed CMSNS. Each curve corresponds to 1, 2, and 3 layers of G–M. (c) Optical microscope image of the annealed CMSNS contacted to 6 electrodes.

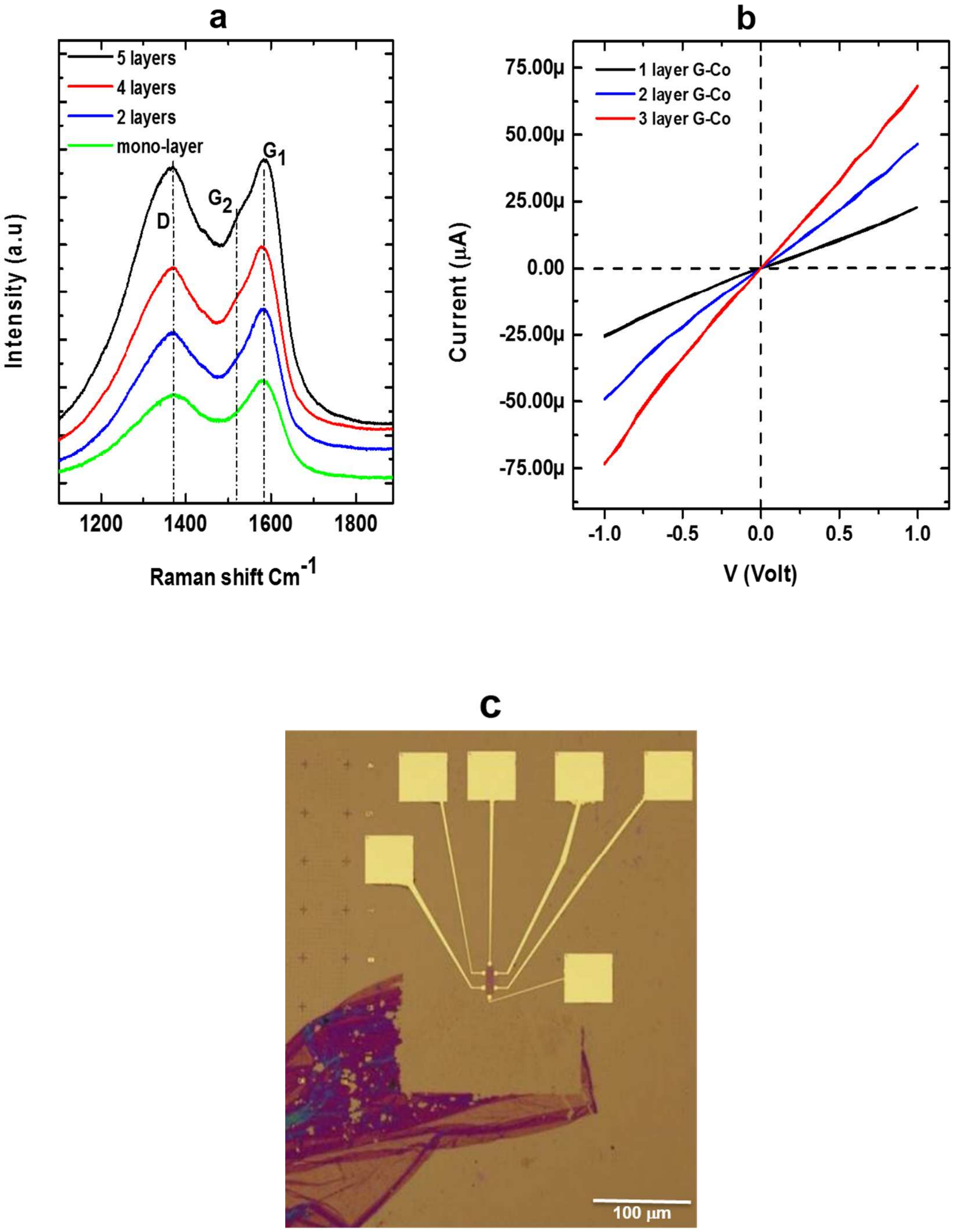

Figure 9. TEM and elemental map of the annealed C-Ni-S-NS. (a) High-resolution TEM micrograph of the annealed CNiSNS deposited on the TEM grid, (b and c) TEM and elemental map of sulfur (red), and nickel (green) of the annealed CNiSNS, (c) High resolution image showing lattice planes of Ni NP, (d) selected area electron diffraction pattern of the Ni NP.

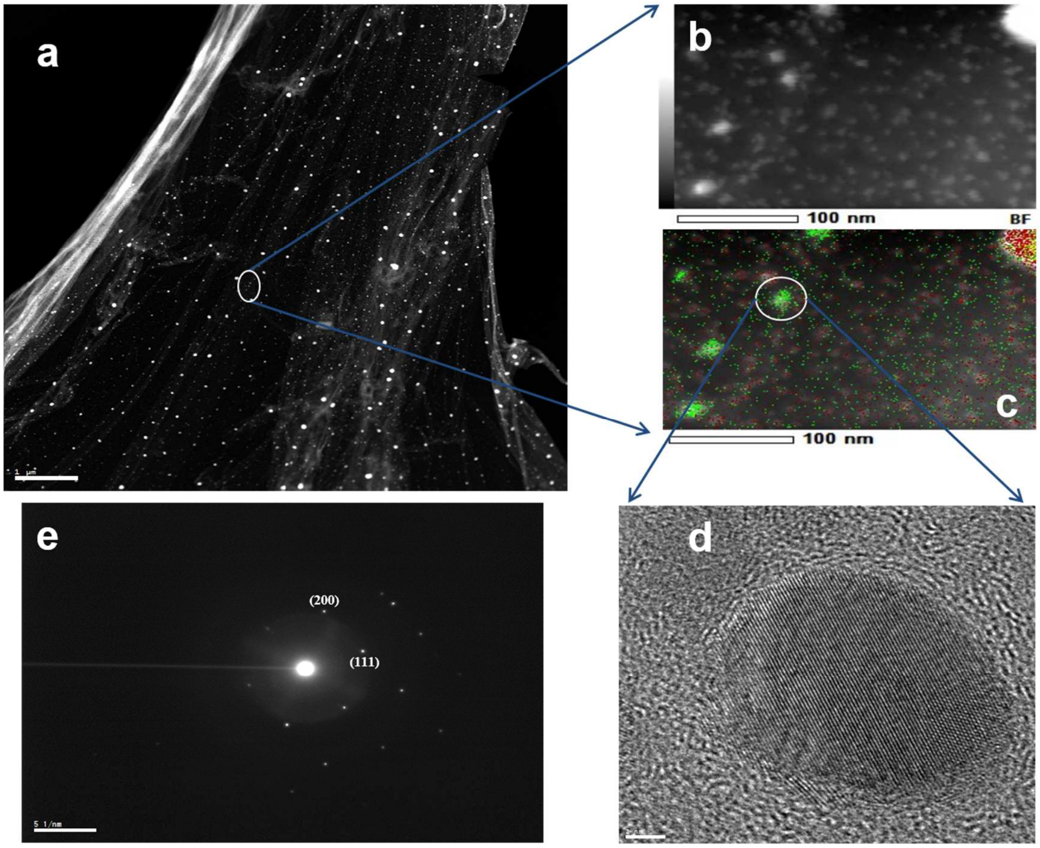

Table of contents entry

In this paper, the author developed a new method to synthesize a metal–sulfide graphene nanosheets (MSGH) starting from a water-hexane interface.